

Preparation of TiO₂ bionic superhydrophobic surface on AZ31 and its anti-corrosion properties

X. Yu^{*}, M. Zhao, R. Li, J. Wang

^a*School of Additive Manufacturing, Zhe Jiang Institute of Mechanical & Electrical Engineering, Hangzhou, China, 310053*

^b*College of Materials Science and Chemical Engineering, Harbin Engineering University, Harbin, China, 150001*

Superhydrophobic surface containing TiO₂ was prepared on the surface of AZ31 magnesium alloy by two-step method. The morphology and composition of the film were characterized by SEM, XRD and FT-IR. The physical and chemical stability of the film was investigated by friction and wear test and contact angle test under different conditions. In addition, self-cleaning performance and corrosion resistance of the film were studied. The results showed that the superhydrophobic surfaces have good resistance to ultraviolet light, acidic and alkaline liquids, which prove that good mechanical stability and chemical stability.

(Received February 22, 2021; Accepted May 28, 2021)

Keywords: Superhydrophobic surfaces, Titanium dioxide, Corrosion resistance, Mechanical stability, Stearic acid

1. Introduction

In recent years, magnesium alloy, as a new material with high specific strength, low density and lightweight, has been widely used in automobile industry [1], auto parts [2] and aviation and navigation industry [3]. As a biodegradable material, magnesium alloy has drawn attention of many biological and medical researchers [4]. Also, its appropriate strength and toughness render it an excellent material for carrying plastic surgical implants and coronary stents [5,6]. However, magnesium is an active metal, which can easily react with oxygen and water vapor to produce magnesium oxide and magnesium hydroxide in the air. This reaction is spontaneous and irreversible. The oxide or hydroxide layer on the surface of magnesium alloy is loose and porous, and the corrosion products cannot prevent the occurrence of corrosion reaction when contacting with humid or corrosive environment [7,8]. In addition, the composition of magnesium alloy is uniform, and the second phase elements or impurities can form corrosion couple with magnesium in the magnesium alloy. The chemical potential of magnesium alloy is lower, and it often acts as anode in the reaction, resulting in galvanic corrosion [9]. The poor corrosion resistance of magnesium alloy makes the unprotected magnesium alloy lose its mechanical properties before the end of its expected service life.

* Corresponding author: yygdupt_mmc@126.com

At present, some progress has been made towards improving the corrosion resistance of magnesium alloys. Through rapid cooling treatment of magnesium alloy, the uniformity of internal structure and composition of magnesium alloy was improved, the formation of internal corrosion couple was inhibited, and the corrosion resistance of magnesium alloy was significantly improved [10,11]. In addition, the surface treatment of magnesium alloy is another important anti-corrosion means. There are numerous methods such as micro-arc oxidation[12], surface alloying[13], chemical vapor deposition[14], physical vapor deposition[15], chemical conversion[16] and organic coating[17]. Wei [18] used micro-arc oxidation and sol-gel method to prepare MAO/SiO₂-ZrO₂ composite coating, which completely covered the surface of magnesium alloy with almost no defects. The physical seal acts as a barrier to give corrosion protection. The corrosion current density of the sample declines by two orders of magnitude and the corrosion potential moves forward by 920 mV. Ishizaki[19] prepared MPE protective coating on magnesium alloy surfaces by chemical vapor deposition method. The coating has super hydrophobicity, strong stability and mechanical strength, and also shows high corrosion resistance. Bionics, as a fresh subject, has become a key research direction. Barthlott [20] found that there is a layer of waxy organic matter on the surface of the lotus leaf, which has low surface energy and is composed of organic molecules with a diameter of 1 nm. The epidermis cells of lotus leaf are like papillae of micron scale. The superhydrophobic surface of the lotus leaf is formed. Zachary [21] conducted a more in-depth study on the surface of lotus leaves and found that when the wax on the surface of lotus leaves was artificially removed, the water contact angle on the surface of lotus leaves decreased sharply, and even showed a super hydrophilic state. Jiang [22,23] proposed that there are both essential factors for constructing superhydrophobic surfaces: one is the micro nano-scale rough surface structure, the other is the low surface energy, both of which are indispensable. With the continuous development of material preparation technology, researchers can gradually design and control the surface morphology and size of superhydrophobic materials[24,25]. By low surface energy modification, superhydrophobic film can be made on different substrates for many potential applications, such as self-cleaning[26-28] and anti-corrosion[29-31] and so on[32-34]. However, most of superhydrophobic surfaces are relatively fragile and easily damaged by the outdoor environment such as acid rain and organic pollutants, which seriously affects its application. Therefore, the durable superhydrophobic treatment is of great importance to improve the corrosion resistance of magnesium alloy and increase its application range and service life.

In this paper, the superhydrophobic film based on TiO₂ was prepared on the surface of AZ31 magnesium alloy by a two-step method. The first layer of the film was formed by anodizing the treated magnesium alloy substrate; the optimal reaction conditions were determined by changing the anodizing voltage parameters, and then TiO₂ was grown on the anodized layer by hydrothermal method to form the surface micro-nano structure. The superhydrophobic surface was formed after modifying by low surface energy materials. Then the morphology and composition of the film were characterized by SEM, XRD and FT-IR, and the physical and chemical stability of the film was studied by contact angle test. In addition, friction, wear and corrosion resistance of the film was studied.

2. Materials and methods

2.1. Materials

AZ31 Magnesium alloy (composition: Mg, Al 3 wt %, Si 0.08 wt %, Mn 0.38 wt %, Si 0.0135 wt %, Fe 0.0027 wt %, Ni 0.002 wt %, Cu 0.001 wt %), absolute ethanol, acetone were purchased from Tianjin Fuyu Fine Chemical Co., Ltd., sodium oxalate, sodium hydroxide, ethylene glycol, stearic acid were purchased from Aladdin reagent limited

2.2. Method

2.2.1. Surface pretreatment of AZ31

The AZ31 plate was cut into 3 cm × 3 cm × 2 mm square samples, and then ground with 600 mesh, 1000 mesh and 2000 mesh silicon carbide sandpaper step by step to remove the oxide layer on the sample surface and make the surface as smooth as possible without scratches. After cleaning with acetone and anhydrous ethanol for 10 min in the ultrasonic cleaning machine, it was repeatedly washed with deionized water and dried in the oven for standby. Tweezers or gloves should be used for the whole process to prevent oil contamination.

2.2.2. Anodic oxidation treatment of samples

The E3647A DC power supply of Agilent company is used to anodize the magnesium alloy. The specific process parameters are: the cathode is self-made carbon rod electrode, and the anode is magnesium alloy sample. Anodized at 50 °C for 10 min. The effects of different anodizing voltages on the film morphology were discussed. The composition of an electrolyte for anodizing is: sodium oxalate 0.05 mol/L, sodium hydroxide 200 g/L, ethylene glycol 8 ml/L. After anodizing, magnesium alloy samples should be repeatedly cleaned with deionized water in ultrasonic to remove excess sodium hydroxide on the surface. After cleaning with absolute ethanol, it dries in the oven for standby.

2.2.3. Preparation of TiO₂ film by hydrothermal method

Firstly, 48 mg Ti (SO₄)₂ was dissolved in 95 ml deionized water, and 5 ml hydrogen peroxides was added to make the solution clear orange. The anodized samples were immersed in the mixed solution vertically, and then put into the reactor for water heat treatment at 120 °C for 10 h. After the reaction, the sample was repeatedly cleaned with deionized water and dried in air. The samples were then treated at 450 °C for 4 h in a muffle furnace. A layer of TiO₂ film was uniformly adhered on the surface of the sample.

2.2.4. Surface modification of samples

In the process of surface modification, stearic acid was utilized to modify the surface energy of the sample. The sample was completely immersed in 1 wt% stearic acid ethanol solution for 1 h, and then washed repeatedly with anhydrous ethanol. Then, the sample was dried in vacuum at 60 °C for 4 h. The surface of the sample was evenly covered with stearic acid. The overall synthesis diagram of the sample is presented in Fig. 1.

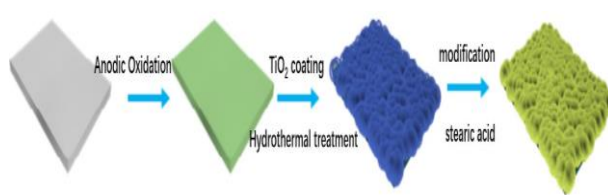


Fig. 1. Schematic diagram for synthesis of superhydrophobic surface.

2.2.5. Characterization

Surface morphology was characterized by scanning electron microscope (SEM, JEOL JSM-6480A). The X-ray diffraction analysis (XRD, Rigaku, Cu K α , $\lambda = 0.15406$ nm, 40 kV, 150 mA, from 5 to 90° at a scanning rate of 10°/min) was carried out at phase the composition and structures of samples. Fourier transform infrared spectroscopy (FT-IR) was used to characterize functional groups of samples. Static contact angles (CA) were carried out on contact angle measurement (Dataphysics). The corrosion resistances of samples were observed by an electrochemical workstation (AutoLAB AUT87412) using the three-electrode system in 3.5 wt % NaCl solution. The sample exposed 1 cm² served as a working electrode (WE), saturated calomel electrode (SCE) was used as reference electrode (RE), a platinum plate was used as counter electrode (CE). Potentiodynamic polarization test was studied from -1 V vs the open circuit potential (OCP) to 1 V vs the OCP at a scan rate of 1 mV/s. The electrochemical impedance spectroscopy test was conducted in OCP, and the frequency range was from 100 kHz to 1mHz with an amplitude of 10 mV.

3. Results and discussion

3.1. Effect of voltage on anodic oxide layer

Anodizing voltages of 5 V, 6 V and 7 V were utilized to pretreat the magnesium alloy respectively. The surface morphology of the samples under the three voltages are presented in Fig. 2b-2d. Compared with surface morphology of untreated magnesium alloy (Fig. 2a), under the anodizing voltage of 5 V, the anodized layer is evenly distributed on the surface of the magnesium alloy substrate, but there are observable cracks on the surface of the sample, which cannot effectively protect the substrate. The cracks on the surface of the sample are obviously reduced under the voltage of 6 V, and there is no large crack through the entire film. In addition, there are also bumps with a diameter of about 5 μ m evenly distributed on the surface, forming the microstructure necessary for superhydrophobic surface. When the voltage reaches 7 V, the surface bulge increases further, and the uniformity of distribution was lost.

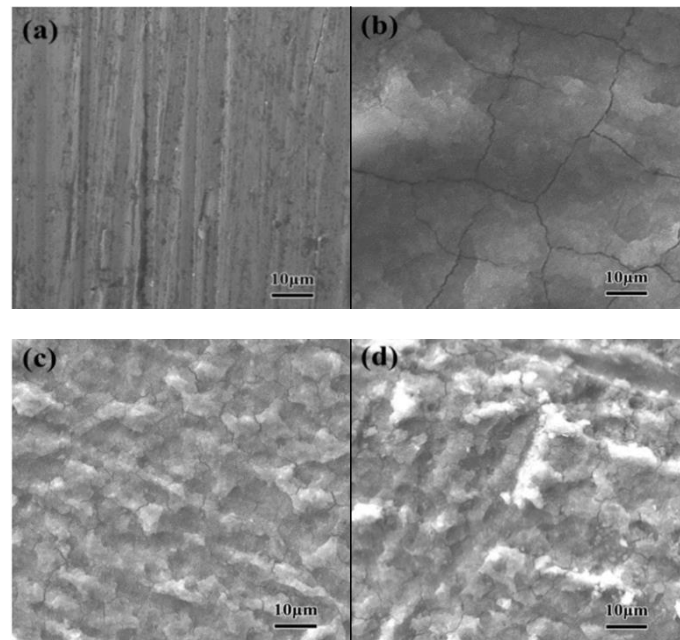


Fig. 2 (a) The surface morphology of pretreated blank magnesium alloy under different anodizing Voltage is (b) 5 V (c) 6 V (d) 7 V.

XRD tests were carried out on magnesium alloy samples under three pretreatment voltages, and the results are displayed in Fig. 3. The diffraction peaks at 34.4° , 36.6° and 47.8° belong to (002), (101) and (102) crystal planes of magnesium alloy substrate, respectively (the standard PDF card # 35-0821). The diffraction peak of $\text{Mg}(\text{OH})_2$ appears at 33° . With the increase of anodizing voltage, the intensity of the diffraction peak also increases. It shows that the thickness of the anodic oxidation film increases. However, it is still very weak compared with the magnesium alloy substrate, which indicates that the thickness of the anodized film is very thin. Founded on the above research, 6 V was selected as the pretreatment voltage.

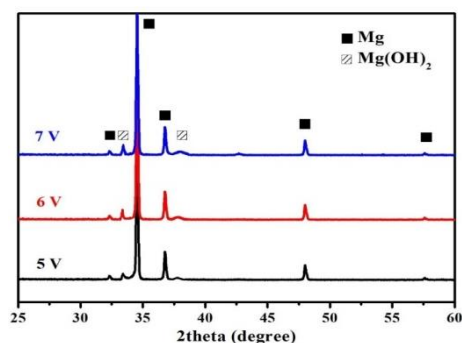


Fig. 3. XRD patterns of samples under different anodizing voltages.

3.2. Effect of anodic oxidation on hydrothermal TiO₂ layer

Most inorganic metal oxides are prepared on the metal substrate by in-situ growth, otherwise it is easy to cause the problem of poor adhesion between the film and the substrate, which greatly limit the selection range of inorganic metal oxides. A layer of hydroxide and oxide on the surface of magnesium alloy by anodic oxidation treatment, which provides favorable conditions for the growth of TiO₂ layer. Fig. 4a shows the surface morphology of the TiO₂ layer grew on the blank magnesium alloy. It can be seen that a small number of TiO₂ particles grow on the surface of the sample, and the combination of the substrate is not very close. After surface modification, the surface morphology of the sample is illustrated in Fig. 4b, we can see that a few micro-nano structures on the surface without TiO₂ particles, which indicates that the adhesion between TiO₂ particles and the substrate is weak. The contact angle test shows that the contact angle is 135.8° which cannot meet the requirements of superhydrophobic surface. Fig. 4c is the surface morphology of the TiO₂ layer grown on the anodized sample. It can be seen that the surface of the sample grow clusters of TiO₂ sheet structure, and the combination with the substrate is relatively close. The growth of the TiO₂ layer is relatively successful. After surface modification, the surface morphology of the sample is given in Fig. 4d. There are abundant micro and nanostructures on the surface of the samples, which create conditions for the formation of superhydrophobic surface. The contact angle test shows that the contact angle of the sample surface is 155.6° which is larger than the requirement of 150° for superhydrophobic surface.

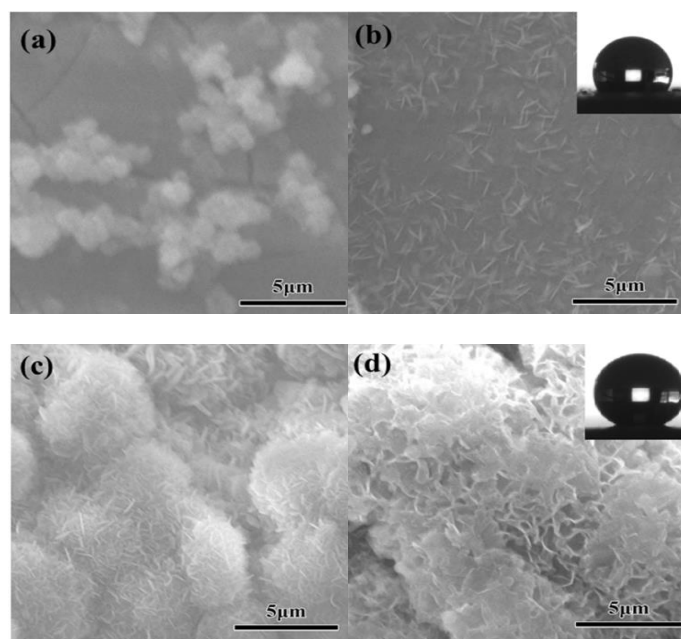


Fig. 4. SEM images and contact angle test of different samples: (a, b) TiO₂ grown on blank magnesium alloy and the contact angle after modified; (c, d) TiO₂ grown on anodized pretreatment samples and the contact angle after modified.

3.3. Chemical composition characterization of superhydrophobic surface

In order to qualify the chemical composition of the superhydrophobic film, the samples were tested by XRD. As shown in Figure 5, line a in the figure is the diffraction curve of anodized magnesium alloy sample, and the diffraction peaks at 34.4° , 36.6° and 47.8° correspond to (002), (101) and (102) crystal planes of magnesium alloy substrate respectively (standard card is PDF #35-0821). The diffraction peak of Mg (OH) 2 appears at 33° . Line b in Fig. 5 shows the diffraction peaks of the samples grown by the hydrothermal method. The peaks at about 24° , 38° , 48° , 54° , 55° and 62.7° correspond to (101), (004), (200), (105), (211) and (204) crystal planes of anatase titanium dioxide respectively (the standard card of TiO_2 is PDF #65-5714), which proves the successful growth of TiO_2 layer.

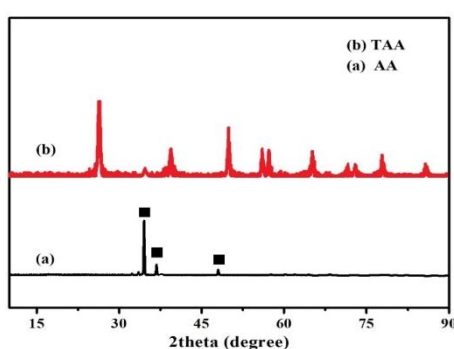


Fig. 5. XRD patterns of different samples: (a) anodized AZ31 (AA) (b) samples with TiO_2 layer on anodized AZ31 (TAA).

The successful preparation of the sample was further supported by FT-IR. Fig. 6 shows the FT-IR spectra of different samples. Fig. 6a shows the infrared spectrum of the sample with hydrothermal grown TiO_2 layer. There is a stretching vibration peak of Ti-O at 605 cm^{-1} . Fig. 6b shows the infrared spectrum of the surface modified sample. As showed in the figure, two peaks were observed at 2916 cm^{-1} and 2870 cm^{-1} due to the stretching vibration of $-\text{CH}_2$ and $-\text{CH}_3$ in stearic acid. In addition, the peak at 1702 cm^{-1} is caused by the stretching vibration of $\text{C}=\text{O}$, three small peaks at 1465 cm^{-1} belong to the bending vibration of $\text{C}-\text{H}$, and the stretching vibration peak at 3450 cm^{-1} belongs to $\text{O}-\text{H}$ disappears. These results indicate that stearic acid has successfully modified the surface of samples.

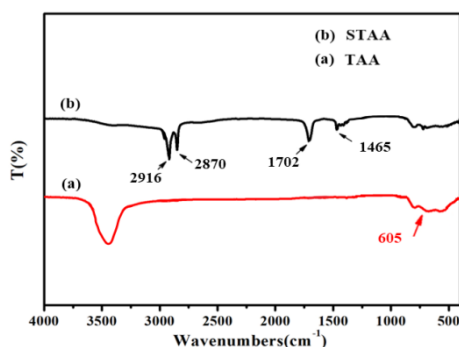


Fig. 6. FT-IR diagrams of different samples: (a) samples of TiO_2 / anodized AZ31 (TAA) (b) samples after modifying by stearic acid (STAA).

3.4. Mechanical stability of superhydrophobic surfaces

In order to verify the mechanical stability of the superhydrophobic film, we used a friction and wear tester to characterize the friction coefficient and mass loss of different samples. The specific parameters of the friction and wear test are as follows: the relative rotation speed between the sample and the ball is 100 r/min, the rotation radius of the ball is 3 mm, the ball material is CCr15 steel, and the load is 150 g. Fig. 7 shows the friction and wear test data of different samples, and Fig. 7a shows the change of friction coefficient with time. The whole friction and wear test were carried out for 20 min. The average value, error and mass loss of the friction coefficient data in 20 min is shown in Fig. 7b. The friction coefficient of treated magnesium alloy substrate is only 0.112, and the value is relatively stable and the fluctuation is small. After 20 min tests, the mass loss is about 1.39 mg, which is mainly due to the smooth surface of magnesium alloy after sanding in the pretreatment of the substrate. After anodizing, the friction coefficient of the sample increases to about 0.149, and the fluctuation range is still lesser. The mass loss is 1.62 mg after 20 min test, which indicate that the surface roughness of the sample increases after anodizing treatment, but the distribution is uniform. After hydrothermal growth of TiO₂ film, the friction coefficient of the sample increases to about 0.18, and the fluctuation range also increases greatly. After 20 min tests, the mass loss is 2.42 mg. It demonstrates that the growth of TiO₂ film can greatly improve the surface roughness of the material. The friction coefficient and mass loss of the superhydrophobic surface modified by stearic acid are slightly larger than those of the magnesium alloy substrate. This is mainly due to the good combination between the TiO₂ layer and the substrate and the extreme hardness of TiO₂, which improves the physical stability of the film, so that the superhydrophobic surface has strong physical stability and is difficult to be worn.

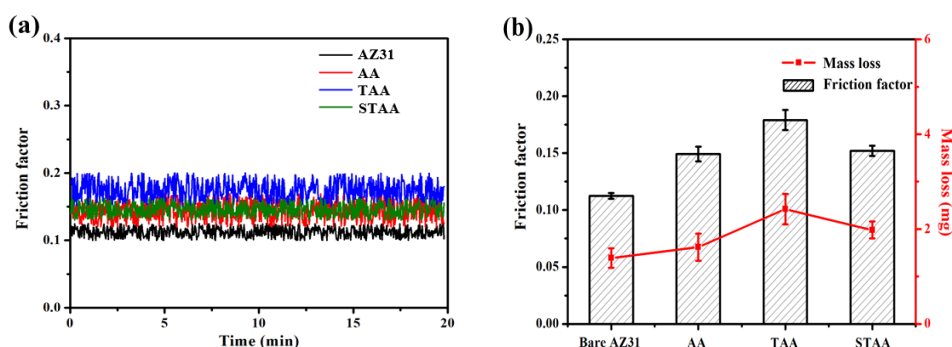


Fig. 7. (a) Variation of friction coefficient with time (b) average value of friction coefficient and mass loss of the sample.

3.5. Chemical Stability of superhydrophobic surfaces

Fig. 8a shows the relationship between the pH value and the contact angle of the droplet. When pH = 1, the contact angle decreases to 156.8 ° and when pH = 13, the contact angle decreases to 156.4 ° which is still greater than 150 °. The results show that the air layer fixed between the micro and nanostructures on the superhydrophobic surface has a good protective effect on the solid surface, and the superhydrophobic surface is not sensitive to acid-base liquids, and its chemical properties are relatively stable. Fig. 8b shows the contact angle of the sample immersed in 3.5 wt% NaCl solution for different time. On the first day of immersion, the contact

angle of the sample decreased dramatically, but it remained stable from the second day. After one week test, the contact angle of the sample is still greater than 155 degrees. The results show that the superhydrophobic surface has superior stability even in corrosive environment. Fig. 8c is a photograph of droplets of different kinds of liquids (ink, milk, coffee and cola) on superhydrophobic surfaces. It can be observed that the composite film is suitable for all kinds of liquids. As showing in Fig. 8d, the contact angle of the sample decreases by about 2° after 7 days of UV irradiation, but it is still much larger than the superhydrophobic surface standard of 150° with a small reduction. When the sliding angle increases from 4.65° to 7° , the film is still superhydrophobic. This demonstrates that the TiO_2 in the film absorbs ultraviolet light, protects the surface modifier of superhydrophobic film, and improves the service life of the film.

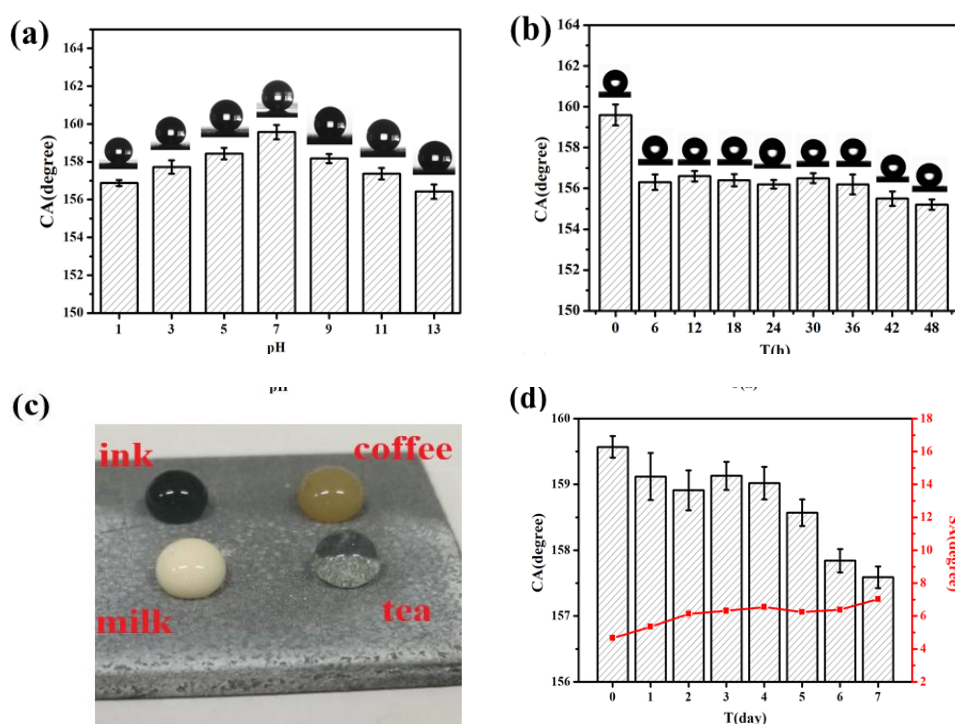


Fig. 8. (a) Effect of droplets with different pH values on contact angle (b) contact angle test of samples immersed in 3.5 wt% NaCl solution for different times (c) hydrophobicity of superhydrophobic surface for different liquids (d) contact angle and sliding angle of samples exposed to ultraviolet light for different times.

3.6. Corrosion resistance of superhydrophobic surface

Fig. 9a shows the potentiodynamic polarization curves of different samples after soaking in 3.5 wt% NaCl solution for 3 h. The test results are summarised in Fig. 9b. It can be seen from the figure that the corrosion potential (E_{corr}) of the blank magnesium alloy substrate is -1.19 V (SCE), and the corrosion current density (i_{corr}) is 7.413×10^{-5} A/cm². Because of the corrosive environment of chloride ion, it can be observed that there are bubbles on the surface of the sample during the test, and hydrogen evolution pitting corrosion has occurred. After hydrothermal growth of TiO_2 film, the corrosion potential moves to -1.44 V (SCE), and the corrosion current density

decreases to $5.37 \times 10^{-7} \text{ A/cm}^2$. This is caused by the formation of a layer of non-conductive magnesium hydroxide on the surface of anodized magnesium alloy. On the one hand, it hinders the occurrence of corrosion, on the other hand, it improves the specific surface area of the sample surface. Hydrophilic magnesium hydroxide affects the wettability of the surface, thus reducing the corrosion potential. The corrosion potential of the samples was -1.49 V (SCE) after a layer of TiO_2 film was coated on the surface of magnesium alloy substrate by hydrothermal method. The corrosion current density is $3.02 \times 10^{-7} \text{ A/cm}^2$, which is not different from that without growth. This is mainly attributable to the fact that TiO_2 is also hydrophilic and has no essential difference from before growth. After stearic acid modification, the corrosion potential of superhydrophobic surface decreased to -1.51 V (SCE) , and the corrosion current density decreased to $3.09 \times 10^{-10} \text{ A/cm}^2$. Compared with the blank magnesium alloy, the corrosion current density decreases greatly, which indicates that the superhydrophobic surface has excellent corrosion resistance.

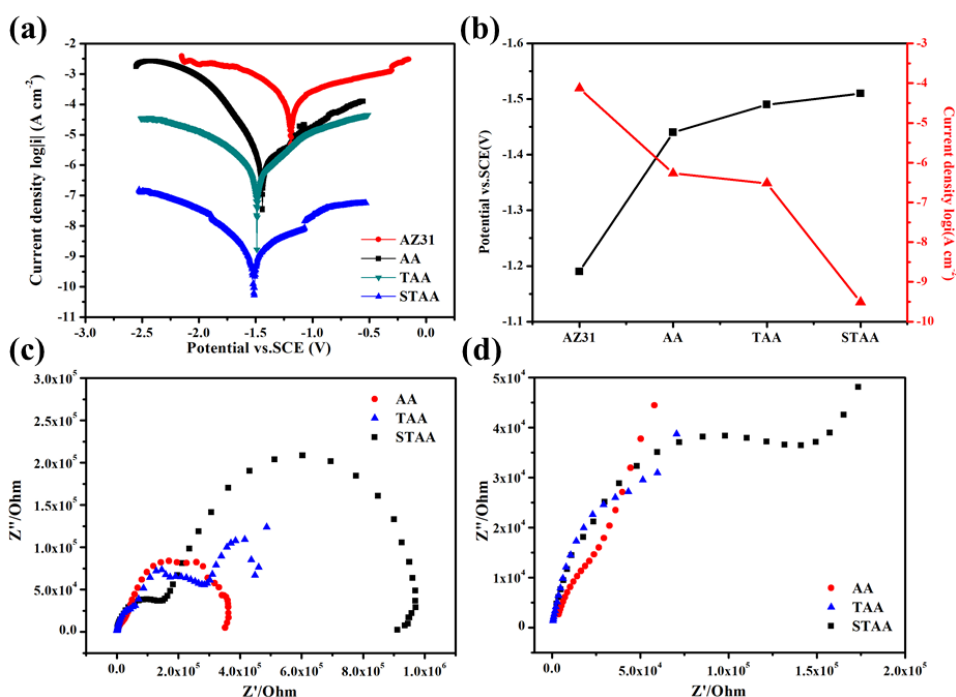


Fig. 9 (a) Potentiodynamic polarization curves of blank AZ31, anodized AZ31 (AA), hydrothermally grown TiO_2 (TAA) and stearic acid modified samples (STAA) (b) corrosion potential and corrosion current data (c) Nyquist diagram of different samples (d) local enlarge in high frequency region.

In order to further analyze the corrosion resistance of superhydrophobic surface, electrochemical impedance spectroscopy (EIS) was utilized to test the corrosion resistance of the samples. Fig. 9c shows the Nyquist diagram of the sample after soaking in 3.5wt% NaCl solution for 6 h, and the high frequency region is locally enlarged in Fig. 9d to show more clearly. The impedance of blank magnesium alloy is below 300Ω . It can be observed in Fig. 9c that the capacitive arc radius of magnesium alloy increases significantly after surface treatment. This indicates that the charge transfer resistance of superhydrophobic surface is very large, and the superhydrophobic surface prevents corrosion by inhibiting the charge transfer.

4. Conclusions

Superhydrophobic surface with a contact angle of 159.6° and a sliding angle of 4.6° was formed on magnesium alloy by two-step method. By changing the voltage parameters of anodic oxidation and characterizing the surface morphology of the samples under different voltages, the optimal reaction voltage of anodic oxidation is 6 V. The friction coefficient of superhydrophobic surface is about 0.152. After 20 min tests, the mass loss is about 1.98 mg, which indicates that the superhydrophobic surface has good mechanical stability. The contact angle of superhydrophobic surface is still more than 150° after being exposed to ultraviolet light for one week.

The superhydrophobic surface is hydrophobic to both acidic and alkaline liquids, indicating that the superhydrophobic surface has superior chemical stability. The corrosion resistance of superhydrophobic surface was investigated by polarization curve test and electrochemical impedance test. Compared with the blank magnesium alloy, the corrosion current of superhydrophobic surface decreases by 4 orders of magnitude. It shows that the superhydrophobic surface has superior anti-corrosion performance and protects the magnesium alloy substrate.

Acknowledgements

This research was supported by Research Fund of Zhe Jiang Institute of Mechanical & Electrical Engineering (A—0271—20—211).

References

- [1] V. R. Abalymov, J. A. Kleymenov, T. N. Drozdova, N. V. Okladnikova, V. P. I. Zhereb, *Journal of Siberian Federal University. Engineering and Technologies*, **8**, 948 (2015).
- [2] T. Prosek, A. Nazarov, F. Goodwin, D. Thierry, *Surf. Coat. Technol.* **306**, 439 (2016).
- [3] J. Villafuerte, D. Wright, *Adv. Mater. Processes* **168**, 53 (2010).
- [4] P. Makkar, S. K. Sarkar, A. R. Padalhin, B. G. Moon, B. T. Lee, *Journal of Applied Biomaterials & Functional Materials* **16**, 126 (2018).
- [5] M. P. Staiger, A. M. Pietak, J. Huadmai et al., *Magnesium and Its Alloys as Orthopedic Biomaterials: A Review*. *Biomaterials* **27**, 1728 (2006).
- [6] J. Wang, J. Tang, P. Zhang et al., *Journal of Biomedical Materials Research Part B Applied Biomaterials* **100B**, 1691 (2012).
- [7] B. Zhang, X. Zhao, Y. Li, B. Hou, *RSC Advances* **6**, 35455 (2016).
- [8] Y. Zhang, C. Blawert, S. Tang et al., *Corrosion Science* **112**, 483 (2016).
- [9] S. Atrens, G. L. Song, L. Ming et al., *Advanced Engineering Materials* **17**, 400 (2015).
- [10] G. L. Song, A. Atrens, *Advanced Engineering Materials* **5**, 837 (2003).
- [11] G. Ballerini, U. Bardi, R. Bignucolo, *Corrosion Science* **47**, 2173 (2003).
- [12] M. Zhang, R. Chen, X. Liu et al., *Journal of Alloys and Compounds* **818**, 152875 (2020).
- [13] D. Lu, X. Ma, Y. Huang, F. Ma, J. Duan, B. J. Hou, *Phys. Chem. C* **123**, 24461 (2019).
- [14] Y. X. Gan, A. S. Hamdan, J. B. Gan, M. Li, *Coatings* **7**, 164 (2017).
- [15] H. Wang, X. Song, L. You, B. Zhang, *Journal of Crystal Growth* **432**, 78 (2015).

- [16] M. A. Hafeez, A. Farooq, A. Zang et al., *J Coat Technol Res* **17**, 827 (2020).
- [17] L. Bromberg, X. Su, K. R. Phillips, T. Alan Hatton, *Ind. Eng. Chem. Res.* **57**, 10992 (2018).
- [18] S. Wei, B. Chen, X. Shi et al. *Journal of Alloys & Compounds* **474**, 541 (2009).
- [19] T. Ishizaki, J. Hieda, N. Saito et al. *Electrochimica Acta.* **55**, 7094 (2010).
- [20] W. Barthlott, C. P. Neinhuis, *Planta* **202**, 1 (1997).
- [21] Z. Burton, B. Bhushan, *Ultramicroscopy* **106**, 709 (2006).
- [22] W. S. Wong, G. Liu, A. Tricoli, *Small* **13**, 14 (2017).
- [23] P. Wang, T. Hayashi, Q. Meng, Q. Wang, H. Liu, *Small* **13**, 4 (2017).
- [24] X. Zhang, F. Shi, J. Niu et al., *Journal of Materials Chemistry* **18**, 621 (2008).
- [25] P. Roach, N. J. Shirtcliffe, M. I. Newton, *Soft Matter* **4**, 224 (2008).
- [26] H. Yoon, H. Kim, S. S. Lathe, M. W. Kim, S. Al-Deyab, S. S. Yoon, *J. Mater. Chem. A* **3**, 11403 (2015).
- [27] M. Toma, G. Loget, R. M. Corn, *ACS Appl. Mater. Interfaces* **6**, 11110 (2014),
- [28] J. E. George, V. R. M. Rodrigues, D. Mathur, S. Chidangil, S. D. George, *Mater. Des.* **100**, 8 (2016).
- [29] C. Wu, Q. Liu, R. Chen, J. Liu, H. Zhang, R. Li, K. Takahashi, P. Liu, J. Wang, *ACS Appl. Mater. Interfaces* **9**, 11106 (2017)
- [30] B. Zhang, X. Zhao, Y. Li, B. Hou, *RSC Advances* **6**, 35455 (2016).
- [31] Y. Zhang, C. Blawert, S. Tang, J. Hu, M. Mohedano, M. L. Zheludkevich, K. U. Kainer, *Corros. Sci.* **112**, 483 (2016).
- [32] Y. S. Li, H. Shao, P. F. Lv, C. Y. Tang, Z. K. He, Y. L. Zhou, M. B. Shuai, J. Mei, W. M. Lau, *Chem. Eng. J.* **338**, 440 (2018).
- [33] H. Xu, A. Clarke, J. P. Rothstein, R. J. Poole, V. J. *Colloid Interface Sci.* **513**, 53 (2018).
- [34] P. W. Wang, T. Y. Zhao, R. X. Bian, G. Y. Wang, H. R. Liu, *ACS Nano* **11**, 12385 (2017).